JOURNAL OF THERMOPHYSICS AND HEAT TRANSFER
Vol. 12, No. 2, April–June 1998

Turbulence Structure of Heat Transfer Through a Three-Dimensional Turbulent Boundary Layer

Douglas J. Lewis* and Roger L. Simpson†
Virginia Polytechnic Institute and State University, Blacksburg, Virginia 24061

The structure of turbulent heat transfer in the well-documented pressure-driven, three-dimensional turbulent boundary layer generated by a wing–body junction was studied experimentally using a constant-current resistance thermometer and a fast-response, thin-layered surface heat flux gauge. Simultaneous time-resolved surface heat flux and temperature profile measurements were taken in the spatially developing three-dimensional turbulent boundary layer upstream of the wing. Mean heat transfer was decreased by three dimensionality. Mean temperature profiles showed logarithmic behavior but did not collapse on a law-of-the-wall profile. Statistical and spectral analyses of the temperature fluctuations provide information on changes to the near-wall turbulent structures. The strength of ejections from the near-wall region was decreased by three dimensionality. Time-delayed correlations of the surface heat flux and flow temperature revealed an initially linear turbulent wave front whose inclination angle increases with three dimensionality. Coherency between wall heat flux and temperature fluctuations in the outer boundary layer was decreased by three dimensionality.

Nomenclature

C_p = specific heat
F_θ = flatness factor of normalized temperature fluctuations, $\overline{\theta^4}/(\overline{\theta^2})^2$
f = frequency, Hz
$G_{qt}(f)$ = cross-spectral density of flow temperature and surface heat flux
$G_{tt}(f)$, $G_{qq}(f)$ = autospectral density of flow temperature and surface heat flux
$\boldsymbol{H}$ = enthalpy thickness vector
h = convection film coefficient, W/(m^2 K)
L_γ = coherence length scale
Pr = Prandtl number
Pr_t = turbulent Prandtl number, $\varepsilon_m/\varepsilon_h$
q = heat flux, W/m^2
$Re_{(\,)}$ = Reynolds number based on length scale ( )
$R_{q\theta}(\tau)$ = time-averaged correlation coefficient between q and θ at time shift τ
St = Stanton number, $h/(\rho C_p U_\infty)$
S_θ = skewness factor of temperature fluctuations, $\overline{\theta^3}/(\overline{\theta^2})^{3/2}$
s = distance measured along path connecting measurement locations
T = local time-averaged temperature
T_w = wall temperature
T^+ = temperature in inner variables, $(\Theta/St)/(U_\tau/U_\infty)$
T_∞ = freestream temperature
t = time
U, V, W = local time-averaged velocity components in x, y, and z directions, respectively
U_τ = inner velocity scale, $U_\infty(\tau_w/\rho)^{1/2}$
U_∞ = time-mean velocity at edge of boundary layer
u, v, w = fluctuating velocity components in x, y, and z directions, respectively
x, y, z = wind-tunnel coordinates, Fig. 2
y^+ = $y\rho U_\tau/\mu$
α = inclination angle of turbulent wave front
β_{FS} = angle between local freestream direction and tunnel axis
β_H = angle between enthalpy thickness vector direction and tunnel axis
β_{WS} = angle between local wall shear-stress direction and tunnel axis
γ^2 = spectral coherency between surface heat flux and temperature
δ = boundary-layer thickness, $U/U_\infty = 0.995$
δ_T = thermal boundary-layer thickness, $\Theta = 0.995$
ε_h = turbulent diffusivity for heat transport, $\overline{v\theta}/(\partial\Theta/\partial y)$
ε_m = kinematic eddy viscosity for two-dimensional boundary layer, $-\overline{uv}/(\partial U/\partial y)$
$|\varepsilon_m|$ = magnitude kinematic eddy viscosity used for three-dimensional boundary layer, Eq. (3)
Θ = local time-averaged normalized temperature, $(T_w - T)/(T_w - T_\infty)$
θ = fluctuating temperature component of Θ
θ' = rms value of θ
μ = viscosity, m^2/s
ρ = density, kg/m^3
τ = time shift
τ_w = wall shear-stress magnitude

Received May 14, 1997; revision received Sept. 30, 1997; accepted for publication Oct. 3, 1997.

*Research Assistant, Department of Aerospace and Ocean Engineering; currently Aerospace Engineer, U.S. Naval Surface Warfare Center, Dahlgren Division, Dahlgren, VA 22448. E-mail: djlewis@nswc.navy.mil. Member AIAA.

†Jack E. Cowling Professor, Department of Aerospace and Ocean Engineering. E-mail: simpson@aoe.vt.edu. Fellow AIAA.

Introduction

THREE-dimensional turbulent boundary layers (TBLs) occur in many practical applications where convective heat transfer is significant. Flow in a gas–turbine engine is one well-known example. It is well known that, in three-dimensional flows, the turbulence structure is significantly different from that observed in two-dimensional boundary layers. Much of the research has focused on the changes in turbulent momentum transport in unheated three-dimensional flows.[1,2]

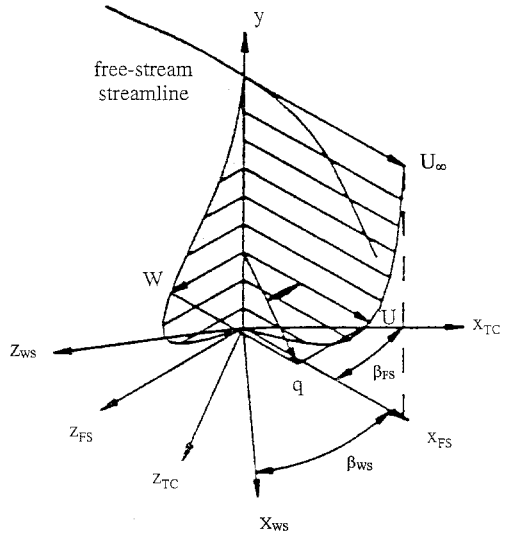

Fig. 1 Sketch of a typical velocity profile in a three-dimensional turbulent boundary layer and definitions of coordinate systems used: TC = tunnel coordinate system, FS = local freestream coordinate system, and WS = local wall-stress coordinates.

Significantly less attention has been paid to the turbulent transport of thermal energy for simple three-dimensional flows. Although there are global heat transfer measurements for such cases, no detailed studies of the relationships between the fluid turbulence and the heat transfer have been made.

The mean flowfield in a three-dimensional TBL is characterized by a flow direction that varies with distance from the wall (Fig. 1). The changing direction of the flow with distance from the wall results in some features that are distinctly different from two-dimensional TBLs. Mean velocity profiles do not collapse onto a single law-of-the-wall profile.[3,4] The mean turbulent shearing-stress direction generally lags the mean velocity gradient direction, so that an isotropic eddy viscosity model cannot reflect the correct physics of the stress-producing structures.[3,5] Also, there is a decrease in the ratio of the shear stress to twice the turbulent kinetic energy.[3,6] This decrease suggests a decrease in the ability of the three-dimensional TBL to transfer momentum and heat.

Many of the observed differences between two- and three-dimensional TBLs are thought to be the result of changes in coherent structures in the boundary layer. These coherent structures consist of the well-documented low-speed streaky structures in the sublayer and the quasiperiodic sweep–ejection sequence, which consists of ejections of low-speed fluid from the near-wall region followed by sweeps of high-speed fluid from the outer layer and log regions.[7] The majority of turbulence production in the entire boundary layer is known to occur in the buffer region during this sweep–ejection cycle.[8] Several recent experiments reported changes in the coherent structure in three-dimensional TBLs. In summary, the near-wall flow is more organized,[9] the strength of the near-wall sweep–ejection motions is decreased,[10] the frequency of the sweep–ejection motions is decreased,[11] and the interaction between the inner and outer regions is decreased[12] by three dimensionality.

Few heat transfer experiments have been made in simple spatially developing three-dimensional boundary layers. Abrahamson and Eaton[13] reported mean surface heat flux and temperature profile measurements in the spatially developing pressure-driven three-dimensional TBL upstream of 60- and 90-deg wedges. They found that the mean surface heat transfer decreased with distance downstream faster in a three-dimensional boundary layer than in a two-dimensional boundary layer and that this decrease was greater with stronger three dimensionality. Abrahamson and Eaton proposed that the heat transfer correlates with a Reynolds number based on the magnitude of an enthalpy thickness vector.

The purpose of the present study is to examine the effects that the changes in turbulence structure caused by three dimensionality have on heat transfer. The case studied here was the spatially developing pressure-driven three-dimensional TBL upstream of a wing–body junction formed by a modified NACA 0020 wing and a flat plate. The fluid mechanics of this test flow are extremely well documented from previous studies.[3–6,9,14–16] This test case differs from many other experimentally examined three-dimensional flows in that the mean flow variables depend on three spatial axes rather than two axes, such as flows in which the three dimensionality of the flow has been generated either by a rotating cylinder or by a spanwise pressure gradient in one direction only throughout the flow. For these degenerate three-dimensional flows, a local near-wall equilibrium exists that causes the mean velocity profiles to be self-similar in wall-shear-stress coordinates.[17,18] Ölçmen and Simpson[4] found that a universal law of the wall exists only for the beginning stages of three-dimensional flow. This is the result of the inner and outer regions coming from different directions and having different histories, i.e, the sweeps from the outer region and the ejections from the inner region are not related.[17]

Experimental Apparatus and Procedure

Test Facility

Only a brief description of the experimental facilities and instrumentation will be given here. A more detailed description of the experimental setup may be found in Ref. 19. The measurements were carried out in the Virginia Tech Aerospace and Ocean Engineering Low Speed Boundary Layer Tunnel. The test section is 6 m long and 0.91 m wide. In the absence of the wing, the test section produces a two-dimensional, zero-pressure-gradient turbulent boundary layer on the floor of the test section. The inlet flow is tripped by the 0.63-cm blunt leading edge of the tunnel floor to ensure that the boundary layer is turbulent. Flow entering the test section is subjected to a 1.5:1 contraction produced by the shape of the upper wall. A throat is reached 1.63 m downstream of the entrance, where the section is 254 mm in height. Downstream of the throat, the upper wall is almost parallel to the flat lower wall, diverging gradually from it with distance downstream to account for boundary-layer growth.

To study heat transfer, a false floor was placed in the tunnel. The false floor is made of five sections of 1.59-cm-thick aluminum plate and rests with its upper surface 34.9 mm above the test section floor. Silicone-rubber-insulated electric resistance heaters are secured to the bottom of the floor using room-temperature-vulcanized silicone adhesive. The heaters are insulated from beneath by a 1.9-cm-thick styrofoam sheet. Copper–constantan 0.5106-mm-diam thermocouples are soldered into a 3.18-mm-diam brass tube and press-fit into the aluminum floor for feedback control. Power to the heaters is controlled by five Eurotherm 810 three-mode process controllers, each connected to a Eurotherm 831 silicon-controlled rectifier power supply. The automatic controllers hold the surface temperature constant and uniform to within $\pm 0.5°C$.[19] The aluminum floor of the tunnel is heated from a distance 121.9 cm downstream of the test section entrance, for a distance of 335.3 cm.

The test flow was generated by mounting a model wing at zero angle of attack and zero sweep on the test section floor, with its leading edge 1.8 m downstream of the beginning of the heated floor section. Inserts for the wind-tunnel sidewalls were used to minimize blockage-induced pressure gradients around the vertical wing.[19] The model wing consists of a 3:2 elliptical nose joined to a NACA 0020 tail at its maximum thickness. The model was made of aluminum and was heated with silicone-rubber-insulated electric resistance heaters epoxied inside the models. The flow over the model was tripped

with a strip of 120-grade sandpaper to prevent unsteadiness from natural flow transition.

Heat Flux Measurement

A model HFM-6 heat flux microsensor (Vatell Corp.) was used to measure surface heat flux. The heat flux microsensor (HFM) consists of several thin-film metal layers that form a differential thermopile across a thin thermal resistance layer. The sensing area is 4 by 6.5 mm. The layers of the gauge are sputter-coated onto a 2.54-cm diam, 6.35-mm-thick aluminum nitride disk. Feedthrough leads are used to bring the signal through the substrate. The thin construction of the gauge (<2 μm) is physically unobtrusive in the flow and causes minimal disruption of the flow or the thermal boundary layer. The HFM has a flat electronic frequency response up to 50 kHz and produces a continuous voltage linearly related to the heat flux.[20] A platinum resistance temperature sensor (RTS), sputter-coated onto the aluminum nitride disk near the heat flux sensor, measures gauge surface temperature. A Vatell Corp. differential amplifier was used to provide a small constant current to the RTS and to amplify the RTS output voltage. Potentiometers on the amplifier were used to null the heat flux and RTS temperature output. Calibration of the HFM is described in Ref. 19.

Temperature Measurement

Flow temperature was measured using a hot-wire anemometer operating in the constant-current mode. The probe used was a custom-made Thermo Systems 1261A-P.5 miniature boundary-layer probe with a 1.25-μm-diam × 0.5-mm-length platinum wire. A Dantec 56C01 anemometer with a Dantec 56C20 bridge was used to provide a constant 0.2-mA current to the probe. The wire length corresponds to 26 viscous units ($\mu/\rho U_\tau$) in the approach boundary layer. The small wire diameter provides an upper frequency limit of approximately 2 kHz at all velocities and turbulence intensities of interest.[19] No correction was made to account for low-frequency attenuation of the cold-wire signal as a result of conduction to the support needles. Bremhost and Gilmore[21] showed that, for a platinum wire with a length-to-diameter ratio of 400, the error introduced by assuming a flat frequency response up to the corner frequency is approximately 5%.

Experimental Technique

The freestream temperature in the wind tunnel was held constant at 25 ± 1°C, and the floor of the tunnel was held constant and uniform at 45 ± 0.5°C. The nominal airspeed at the test section throat upstream of the wing was 27.5 m/s, and the momentum thickness Re_θ, measured 228.6 mm upstream of the nose of the wing with the wing in place, was 6.96×10^3.

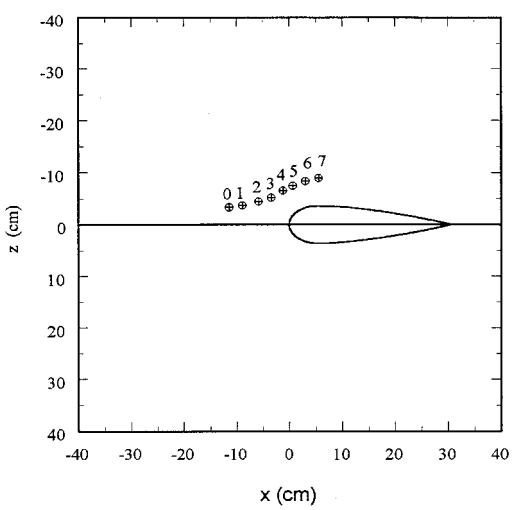

Fig. 2 Plan view of measurement locations relative to the wing.

Table 1 Flow characteristics at each measurement station[a]

Station	X_{TG}, mm	Z_{TG}, mm	U_∞, m/s	β_{FS}, deg	β_{WS}, deg	δ mm	U_τ, m/s
0	−114.0	−33.4	26.3	1.68	6.1	38.6	0.92
1	−88.8	−36.8	24.9	2.64	11.5	39.2	0.87
2	−58.1	−44.5	24.8	4.81	24.0	40.2	0.87
3	−33.7	−51.7	25.3	8.63	33.7	39.3	0.96
4	−12.0	−65.6	27.3	9.45	30.6	39.0	1.11
5	6.6	−74.7	29.5	7.71	19.7	39.6	1.15
6	30.3	−83.7	30.5	5.09	7.2	39.2	1.16
7	55.1	−89.7	31.0	2.71	3.5	38.8	1.20

[a]From Ölçmen and Simpson.[5]

Surface heat flux and temperature profiles were measured at eight locations (Fig. 2), where Ölçmen and Simpson made three-component velocity measurements using a fiber-optic laser-Doppler velocimeter.[5] Following Ölçmen and Simpson the locations will be referred to as stations 0 through 7, starting with the most upstream location. These stations lie along a line determined by the mean velocity vector component parallel to the wall, at a location in the layer where the $\overline{u^2}$ kinematic normal stress is maximum. The measurement locations, in tunnel coordinates, and the important flow parameters at the measurement stations are given in Table 1. The tunnel coordinate system is defined as having the x axis parallel to the wind-tunnel centerline and positive in the downstream direction. The y axis is normal to the test wall and positive away from the wall. The z axis completes a right-hand coordinate system. The origin of the coordinate system is located at the junction between the wing leading edge and the test section floor.

The cold-wire and heat-flux signals were sampled simultaneously by a Hewlett-Packard (HP) 3562A dynamic signal analyzer. Sixty segments of 2048 samples of each signal were taken at a frequency of 10,240 Hz and recorded on floppy disk for postprocessing. Spectral analysis of the heat flux and temperature signals was performed in real time by the HP 3562A. Two hundred ensemble averages of the heat flux and temperature power spectra, cospectra, and coherence were calculated from segments of 2048 samples of each signal at a sampling frequency of 10,240 Hz and recorded.

Results and Discussion

Mean Surface Heat Transfer and Temperature Profiles

Results from the mean heat flux and temperature profile measurements are summarized in Table 2. Figure 3 shows mean temperature profiles measured at the eight locations plotted in wall coordinates. Directly measured values of shear stress[5,14] and heat flux were used to compute T^+ and y^+. Also shown for comparison is the logarithmic temperature law of the wall

$$T^+ = (1/\kappa_n)\ell n(y^+) + B \tag{1}$$

($\kappa_n = 0.4556$, $B = 3.654$) (Ref. 22), and the molecular conduction sublayer equation

$$T^+ = Pry^+ \tag{2}$$

The profiles collapse only in the sublayer and buffer regions. In the semilogarithmic region, the slope of the profiles decreases from station 0 to 2, and then increases monotonically from stations 2 to 7.

The semilogarithmic temperature profile is the result of a linear variation of ε_h near the wall. An increase in the slope of the temperature profile indicates a decrease in the slope of the ε_h profile. In two-dimensional boundary layers, ε_h is related to ε_m through $Pr_t = \varepsilon_m/\varepsilon_h$. For a three-dimensional boundary layer, we can relate the eddy diffusivity to $|\varepsilon_m|$, which is defined as

Table 2 Heat transfer parameters at each station

Station	$St \times 10^3$	δ_T, mm	H, mm	β_H deg	α, deg
0	1.75	36.0	2.79	2.77	24.7
1	1.88	36.0	2.69	4.68	24.5
2	1.84	37.7	2.95	10.33	28.6
3	1.81	39.7	3.21	16.72	37.9
4	1.80	39.8	3.52	18.04	47.3
5	1.66	41.0	3.33	15.10	41.4
6	1.60	40.9	3.67	10.83	58.0
7	1.53	40.3	3.57	6.80	——

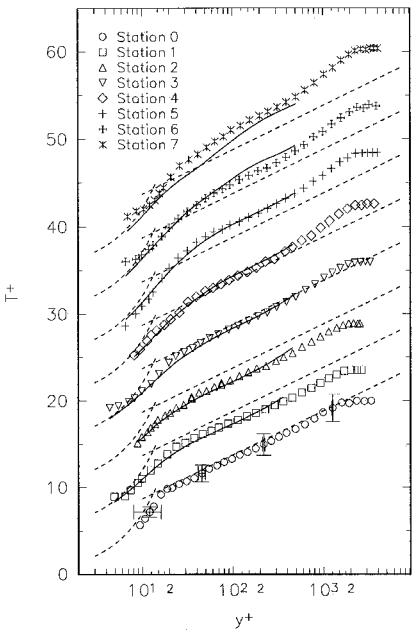

Fig. 3 Mean temperature profiles in wall-law coordinates. *Y*-axis scale applies to the profile at station 0. Remaining profiles are offset successively by 5. - - - - -, show temperature law of the wall [Eq. (1)] and molecular conduction sublayer equation [Eq. (2)]. ——, mean temperature profiles calculated from the magnitude eddy viscosities shown in Fig. 4. Typical uncertainties for T^1 and y^1 are shown for station 0.

the ratio of the magnitude of the total turbulent shear stress to the magnitude of the total strain rate

$$|\varepsilon_m| = \frac{[(-\overline{uv})^2 + (-\overline{wv})^2]^{1/2}}{\left[\left(\frac{\partial U}{\partial y}\right)^2 + \left(\frac{\partial W}{\partial y}\right)^2\right]^{1/2}} \tag{3}$$

The magnitude eddy viscosity is invariant with rotation about an axis perpendicular to the wall.

Figure 4 shows profiles of $|\varepsilon_m|$ at stations 1–7, calculated from the data of Ölçmen and Simpson.[5] The solid line in Fig. 4 is the relation $|\varepsilon_m| = 0.41\ y^+$, which is valid for two-dimensional TBLs. The magnitude kinematic eddy viscosity in the near-wall region decreases from stations 1 to 7. A basic question arises: Is the decrease in ε_h proportional to the decrease in ε_m alone, or is the turbulent Prandtl number also affected by three dimensionality? To answer this question, the near-wall energy equation may be integrated from the wall outward to yield

$$T^+ = \int_0^{y^+} \left(\frac{1}{Pr} + \frac{\varepsilon_h}{\nu}\right)^{-1} dy^+ \tag{4}$$

Equation (4) was numerically integrated by assuming $\varepsilon_h = |\varepsilon_m|/Pr$ and using the measured values of $|\varepsilon_m|$ with $Pr_t = 0.9$. Results are shown as solid lines in Fig. 3. Note that Eq. (4) is valid only in the constant-heat-flux region out to about $y^+ = 300$. At stations 0–6, agreement is very good between the measured and predicted values of T^+. At station 7, the measured values are slightly higher than the predicted values, indicating $Pr_t > 0.9$. However, the difference is within the uncertainty in the measured values of T^+. Therefore, the agreement between the calculated and directly measured temperature profiles suggests that Pr_t is unaffected by three dimensionality. The significance of this is that any turbulence model that correctly predicts the shear stresses $-\overline{uv}$ and $-\overline{wv}$ can be used to predict heat transfer.

Figure 5 is a plot of the development of the Stanton number in the three-dimensional boundary layer. Also plotted in Fig. 5 is the heat transfer coefficient obtained from the two-dimensional zero-pressure-gradient correlation

$$St = 0.0287 Pr^{-0.4} Re_x^{-0.2} \tag{5}$$

where the coordinate x was obtained by matching the measured St in the approach flow upstream of the wing to Eq. (5). The coordinate s in Fig. 5 is defined by the path connecting the measurement locations, with $s = 0$ at the test section entrance. This path is not actually a streamline of either the freestream or near-wall flow but is useful for comparison with the two-dimensional correlation. The Stanton number distribution follows the two-dimensional correlation from station 0 to 4 and then decreases faster than the two-dimensional correlation.

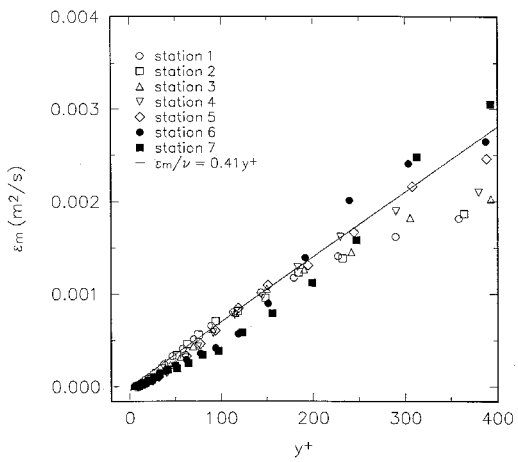

Fig. 4 Near-wall variation of magnitude eddy viscosity. ——, «*m*/ *v* = 0.41y^1; from data of Ölçmen and Simpson.[5]

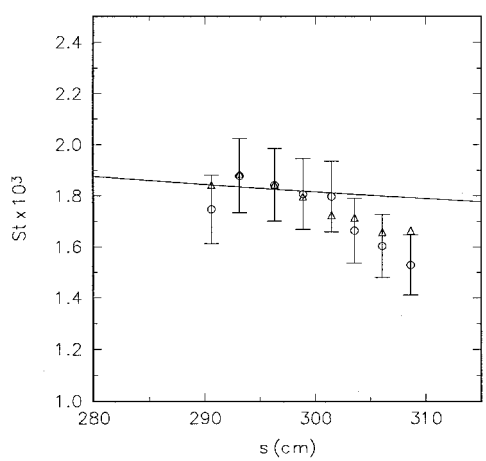

Fig. 5 Stanton number distribution in three-dimensional boundary layer. ○, measured *St* with uncertainty bars; △, calculated from enthalpy thickness vector magnitude and Eq. (7); ——, Eq. (5). Typical uncertainty is *St* 6 7.8%, *Re$_H$*6 9.3%.

Enthalpy Thickness Vector Correlation

For three-dimensional TBLs, Abrahamson and Eaton[13] proposed that heat transfer is related to an enthalpy thickness vector, which for an incompressible constant property flow is defined

$$\boldsymbol{H} = \left[\frac{1}{U_\infty} \int_0^\infty U(1 - \Theta)\, dy,\ 0,\ \frac{1}{U_\infty} \int_0^\infty W(1 - \Theta)\, dy \right] \quad (6)$$

in local freestream coordinates. Abrahamson and Eaton[13] propose that the two-dimensional Stanton number–enthalpy thickness correlation extends to three-dimensional flows using a Reynolds number based on the magnitude of $\boldsymbol{H}$

$$St = 0.125 Pr^{-0.5} Re_H^{-0.25} \quad (7)$$

To calculate the enthalpy thickness vector, the U and W components of the velocity vector measured by Ölçmen and Simpson[5] were fit to piecewise cubic splines and interpolated onto the temperature data set. The interpolated data were then combined according to Eq. (6) and numerically integrated to form the components of $\boldsymbol{H}$. The triangular symbols in Fig. 5 show the Stanton number calculated from the magnitude of the enthalpy thickness vector and Eq. (7). The calculated Stanton number distribution agrees with the measured Stanton numbers within the uncertainty of the measurements. This result disagrees with the case studied by Abrahamson and Eaton,[13] who found that the relationship between St and Re_H did not follow the spatial development of St in either x or s.

Figure 6 shows the relationship between the directly measured Stanton numbers and the Reynolds number, based on magnitude of the enthalpy thickness vector. The data of Abrahamson and Eaton[13] are also included. The three-dimensional data lie very close to the two-dimensional correlation. Note that the two points of Abrahamson and Eaton that lie furthest away from the correlation were attributed by those authors to an unheated starting length effect.[13]

The direction of the enthalpy thickness vector β_H is presented in Table 2, along with the direction of the freestream flow and the wall shear stress. Abrahamson and Eaton[13] show that the enthalpy thickness vector is aligned with the direction of mean thermal energy flux across the boundary layer. In their flow, this direction was aligned with the direction of shear stress at the wall. At stations 0–5, the direction of the enthalpy thickness vector is between the freestream direction and the wall shear-stress direction. A significant amount of enthalpy is convected by the outer flow, so that the enthalpy thickness vector direction is skewed away from the near-wall flow. At stations 6 and 7, the enthalpy thickness vector direction lags both the freestream and wall shear-stress directions. This is caused by transport of enthalpy away from the wing by the middle region of the boundary layer at stations 6 and 7.

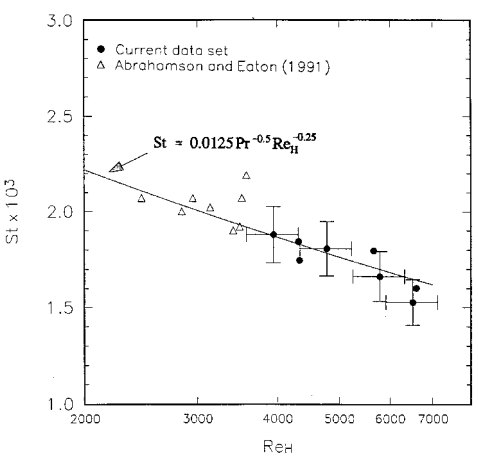

Fig. 6 Correlation between surface heat transfer and magnitude of enthalpy thickness vector. Typical uncertainty is St ± 7.8%, Re_H ± 9.3%.

Statistical Results

Figure 7 is a plot of normalized temperature fluctuation profiles measured at stations 0–6. For all of the stations, the profiles are similar in shape, with the peak value of $\theta' \approx 0.09$ occurring in the buffer region at a y^+ value close to 20.

In two-dimensional boundary layers, the skewness factors of normalized temperature and streamwise velocity histograms attain large positive values in the near-wall region because of the frequent occurrence of sweeps of fluid from the outer region of the boundary layer.[23] In the log region, the histograms become nearly Gaussian ($S_\theta = 0$) because of the equal occurrence and strength of sweeps and ejections. Farther from the wall, the histograms are skewed negatively as a result of increasing frequency of ejections of fluid from the near-wall region.

Figure 8 shows skewness factor profiles of the normalized temperature fluctuations for stations 0–6. Skewness values attain a maximum of 1.0 near $y^+ = 6$ and decrease rapidly through the buffer region. At stations 0–3, the skewness changes sign at approximately $y^+ = 40$. Proceeding further downstream, the location where skewness changes sign increases. At stations 4 and 5, positive skewness values persist through the log region to values of $y^+ = 150$ and 200, respectively. At station 6, the skewness values are not as large near the wall. Moving away from the wall, the skewness decreases more slowly than at the upstream locations and remains at a

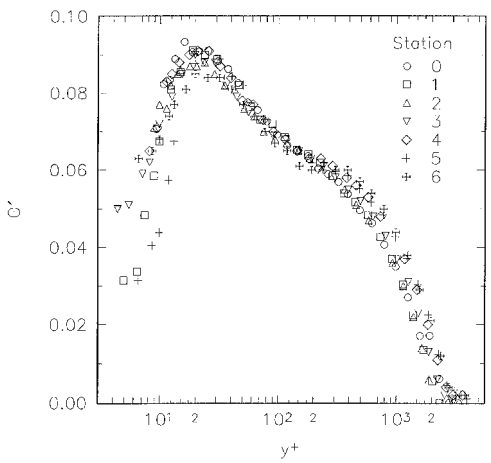

Fig. 7 Temperature fluctuation profiles. Typical uncertainty is u' ± 5%.

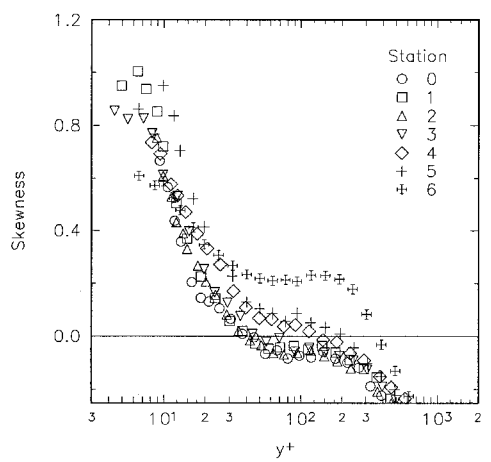

Fig. 8 Profiles of the skewness factor of normalized temperature fluctuations. Typical uncertainty is S_u ± 0.025.

value near 0.2 up to a y^+ value of 300. The positive skewness that develops from stations 3 to 6 may indicate that sweeps of outer-layer cold fluid occur more frequently than ejections of near-wall warm fluid in the region $20 < y^+ < 400$. Another plausible explanation is that sweeps carry a larger relative temperature difference than ejections in this region. From the results of a direct numerical simulation, Sendstad and Moin[10] suggested that mean flow three dimensionality alters the trajectory of the near-wall flow, so that ejections in a three-dimensional TBL originate from a distance farther from the wall and therefore have less momentum and temperature difference.

Figure 9 shows flatness factor (kurtosis) profiles for stations 0–6. For reference, a Gaussian distribution has a flatness factor equal to 3. At stations 0–5, the flatness profiles are very similar to the flatness profiles of temperature and streamwise velocity fluctuations measured in two-dimensional flows.[23,24] Flatness values increase significantly near the wall and at the edge of the boundary layer. Moving away from the wall, flatness values decrease and reach a minimum value near $y^+ = 25$. The flatness values then increase slightly, reaching a local maximum near $y^+ = 100$, and then decrease to a second local minimum at $y^+ = 200$–400.

In a two-dimensional zero-pressure-gradient boundary layer, the first minimum in flatness occurs at the same y location where θ' attains a maximum and skewness becomes zero.[23,24] The temperature flatness factors at stations 0–5 agree with these two-dimensional results. At station 6, the second local minimum is lower than the first minimum. Interestingly, the skewness changes sign at the location of this second minimum,

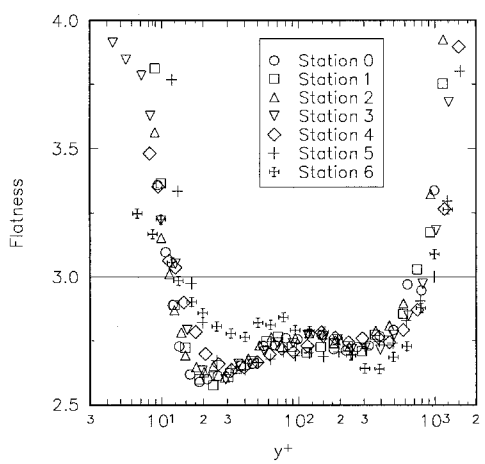

Fig. 9 Profiles of the flatness factor of normalized temperature fluctuations. Typical uncertainty is F_u 6 0.1.

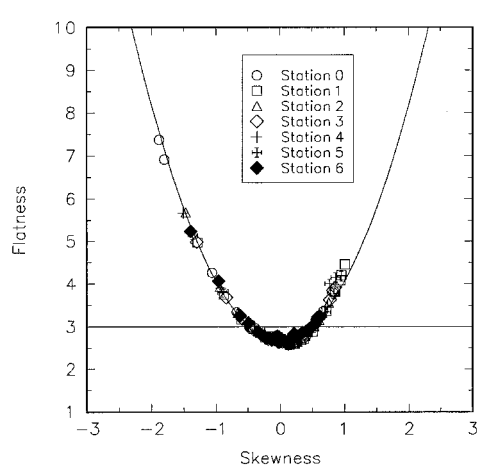

Fig. 10 Plot of flatness factor as a function of skewness factor of normalized temperature fluctuations. ——, parabola fit to the data.

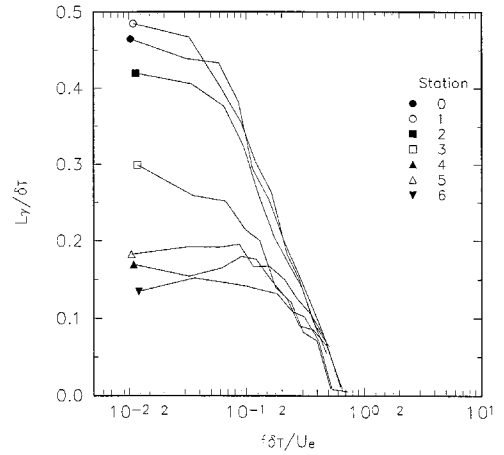

Fig. 11 Effect of three dimensionality on spectral variation of coherence length scale. Uncertainty is L_g/d 6 0.036.

indicating that there may be some relationship between skewness and flatness.

Durst et al.[25] observed that a relationship existed between the flatness and skewness factors of streamwise velocity fluctuations in a two-dimensional zero-pressure-gradient boundary layer. Figure 10 is a plot of the flatness factor as a function of the skewness factor of temperature fluctuations for stations 0–6. A least-squares regression to the data yields

$$F = 1.372S^2 + 2.694 \tag{8}$$

Note that the flatness factor in Eq. (8) attains a minimum value when $S = 0$. Note that this minimum F occurs at the same y locations where $S = 0$ even for station 6, where the skewness factor changes sign far away from the wall.

Coherence Length Scale

Spectral coherency between surface heat flux and flow temperature may be used to define a turbulent length scale. The coherence function between surface heat flux and temperature at a point y in the boundary layer is defined as

$$\gamma^2(f) = \frac{G_{qt}(f)G_{tq}(f)}{G_{qq}(f)G_{tt}(f)} \tag{9}$$

where G_{tt} and G_{qq} are the power spectra of the temperature at location y and the surface heat flux, respectively, and G_{qt} is the cross spectrum between them. The coherency equals 1 for $y = 0$ and decreases as y increases. $L_\gamma(f)$ is then defined as the value of y where the coherence function falls below a statistically significant value. Ha and Simpson[12] chose this critical value as $\gamma_{cr} = 0.27$.

The spectral variation of coherence length scales is presented in Fig. 11 for stations 0–6. The most noticeable feature of this plot is the 50% reduction in coherence length at low frequencies, as the flow progresses downstream from stations 0 to 6. At stations 0–2, the coherency extends to almost half the boundary-layer thickness. At the latter three stations, the coherency extends over only the inner 20% of the boundary layer. The observed decrease in coherency is the result of the flow in the inner and outer regions coming from different directions and having different histories.

Time-Averaged Wave Front of Large-Scale Structures

The shape of the time-averaged wave front of the large-scale structures was estimated using the method described by Brown and Thomas.[26] For each y location where the temperature was

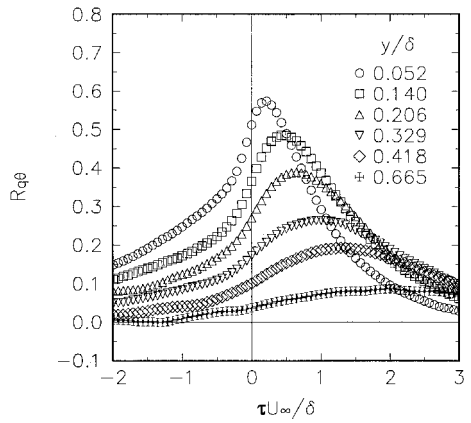

Fig. 12 Long-time average time-delayed correlation coefficient between surface heat flux and temperature at several *y* locations across the boundary layer at station 0.

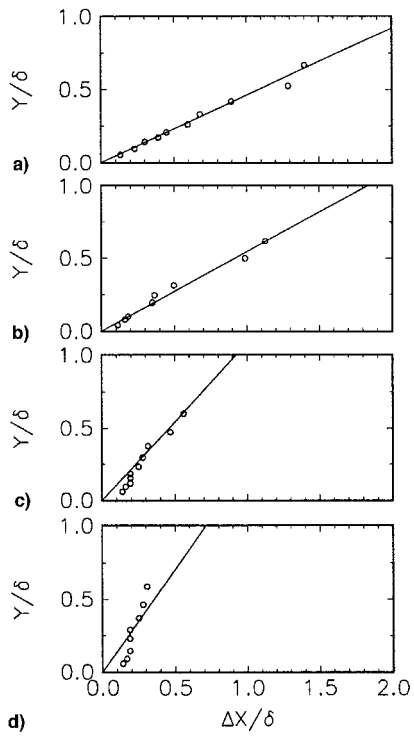

Fig. 13 Time-averaged wave fronts in *x*–*y* plane constructed from time-delayed correlations of surface heat flux and temperature at stations a) 0, b) 2, c) 4, and d) 6.

measured, the long-time averaged correlation coefficient between temperature and surface heat flux, defined

$$R_{q\theta}(\tau) = \frac{\overline{q(t+\tau)\theta(t)}}{\sqrt{\overline{q(t)^2}}\sqrt{\overline{\theta(t)^2}}} \qquad (10)$$

was determined. The results for station 0 are shown in Fig. 12. Note that the peak in the correlation coefficient occurs at increasing time delays τ as the point of temperature measurement moves away from the wall. This is the result of the time delay between large structures hitting the point where temperature was measured and the surface where heat flux was measured. The increasing time delay as y increases implies that the structure is inclined to the wall.

The location of the wave front of the structures at each y location was estimated by assuming that in τ the structures convect downstream a distance ΔX equal to $U_c \times \tau$, where the convection speed U_c was assumed to be $0.7U_\infty$.[26,27] The estimated positions of the wave fronts at the time delay corresponding to maximum correlation coefficient are shown for measurement stations 0, 2, 4, and 6 in Fig. 13. At station 0, the wave front is a straight line inclined at 24.7 deg to the wall. This angle is slightly less than the 30-deg angle measured by Bagheri et al.[27] in a two-dimensional flat-plate thermal boundary layer. As the flow moves downstream and becomes more three-dimensional, the inclination angles increase to values greater than 50 deg. At stations 4, 5, and 6, the wave front is not linear near the wall. Near the wall ($y/\delta < 0.2$), where the surface heat flux and temperature fluctuations are coherent, the wave front is inclined at a smaller angle. This may be the result of overestimating the convection speed in the inner layer, or it could be the result of the structures in the inner layer coming from a different direction than the structures in the outer layer.

Conclusions

Heat transfer in a high-Reynolds-number, pressure-driven, three-dimensional turbulent boundary layer generated by a 3:2 elliptic-nose NACA 0020 tail cylinder protruding from a flat plate was studied experimentally using a constant-current resistance thermometer and a fast-response, thin-layered surface heat flux gauge. Simultaneous time-resolved surface heat flux and temperature profile measurements were taken at eight locations in the spatially developing three-dimensional turbulent boundary layer upstream of the wing. The measurement locations were upstream of the region dominated by the junction vortex.

The time-mean surface heat flux was decreased approximately 10% by three dimensionality. The decrease was attributed to a decrease in the near-wall turbulent eddy viscosity. Profiles of mean temperature suggest that the turbulent Prandtl number is unaltered by three dimensionality. The correlation of Abrahamson and Eaton[13] between mean surface heat flux and Reynolds number, based on the magnitude of an enthalpy thickness vector Re_H, was extended to higher Re_H values by the present data. Profiles of temperature fluctuations changed little with increasing three dimensionality. The skewness and flatness factors of the temperature fluctuations are related by a single quadratic algebraic equation at all stations.

It appears that mean flow three dimensionality reduces surface heat flux by altering the sweep–ejection process in the near-wall region. Positive values of the skewness factor of θ suggest that the strength of ejections of hot fluid from the near-wall region was decreased by mean three dimensionality. This supports the idea that ejections do not penetrate as far into the outer layer in a three-dimensional turbulent boundary layer.

In the early stages of development of three-dimensional flow, time-delayed correlations of the surface heat flux and temperature fluctuations over a range of y locations in the boundary layer indicated the presence of a linear wave front in the x–y plane inclined 25 deg to the wall. As the flow became more three-dimensional, the wave front became nonlinear near the wall, and the inclination angle of the wave front increased. Coherency between the inner and outer regions decreased with mean three dimensionality because the inner and outer regions come from different upstream directions. For low frequencies below $f\delta/U_\infty \approx 0.2$, the coherence length scale is reduced by as much as 0.3δ by the increasing three dimensionality of the flow. Whether or not the breakdown in interaction between the outer and inner regions is responsible for the observed change in the sweep–ejection process is still unclear.

Acknowledgments

This work was supported by the U.S. Air Force Office of Scientific Research under Contract AFOSR-91-0310. H. Helin and Dan Fant were the Program Managers.

References

[1]Anderson, S., and Eaton, J. K., "Reynolds Stress Development in Pressure-Driven Three Dimensional Turbulent Boundary Layers,"

Journal of Fluid Mechanics, Vol. 202, May 1989, pp. 263–294.

[2]Johnston, J. P., and Flack, K. A.,"Review — Advances in Three-Dimensional Turbulent Boundary Layers with Emphasis in the Wall-Layer Region," *Journal of Fluids Engineering*, Vol. 118, No. 2, 1996, pp. 219–232.

[3]Ölçmen, S. M., and Simpson, R. L., "An Experimental Investigation of a Three-Dimensional Pressure-Driven Turbulent Boundary Layer," Virginia Polytechnic Inst. and State Univ., TR VPI-AOE-178, Blacksburg, VA, 1990.

[4]Ölçmen, S. M., and Simpson, R. L., "Perspective: On the Near Wall Similarity of Three-Dimensional Turbulent Boundary Layers," *Journal of Fluids Engineering*, Vol. 114, No. 4, 1992, pp. 487–495.

[5]Ölçmen, S. M., and Simpson, R. L., "An Experimental Study of a Three-Dimensional Pressure-Driven Turbulent Boundary Layer," *Journal of Fluid Mechanics*, Vol. 290, May 1995, pp. 225–262.

[6]Ölçmen, S. M., and Simpson, R. L., "Evaluation of Algebraic Eddy–Viscosity Models in Three-Dimensional Turbulent Boundary Layer Flows," *AIAA Journal*, Vol. 31, No. 9, 1993, pp. 1545–1554.

[7]Kline, S. J., Reynolds, W. C., Schraub, F. A., and Rundstadler, P. W., "The Structure of Turbulent Boundary Layers," *Journal of Fluid Mechanics*, Vol. 30, Pt. 4, Dec. 1967, pp. 741–773.

[8]Kim, H. T., Kline, S. J., and Reynolds, W. C., "The Production of Turbulence near a Smooth Wall in Turbulent Boundary Layer," *Journal of Fluid Mechanics*, Vol. 50, Nov. 1971, pp. 133–160.

[9]Fleming, J. L., and Simpson, R. L., "Experimental Investigation of the Near Wall Flow Structure of a Low Reynolds Number 3-D Turbulent Boundary Layer," AIAA Paper 94-0649, Jan. 1994.

[10]Sendstad, O., and Moin, P., "The Near Wall Mechanics of Three-Dimensional Turbulent Boundary Layers," Stanford Univ., Dept. of Mechanical Engineering, Thermosciences Div., Rept. TF-57, Stanford, CA, 1992.

[11]Flack, K. A., "Near-Wall Structure of Three-Dimensional Turbulent Boundary Layers," *Experiments in Fluids*, Vol. 23, No. 4, 1997, pp. 335–340.

[12]Ha, S., and Simpson, R. L., "An Experimental Investigation of a Three-Dimensional Turbulent Boundary Layer Using Multiple-Sensor Probes," 9th Symposium on Turbulent Shear Flows, Paper 2-3, Dept. of Mechanical Engineering, Kyoto Univ., Kyoto, Japan, Aug. 1993.

[13]Abrahamson, S. D., and Eaton, J. K., "Heat Transfer Through a Pressure-Driven Three-Dimensional Boundary Layer," *Journal of Heat Transfer*, Vol. 113, No. 2, 1991, pp. 355–362.

[14]Ailinger, K. G., "Measurement of Surface Shear Stresses Under a Three-Dimensional Turbulent Boundary Layer Using Oil-Film Interferometry," M.S. Thesis, Dept. of Aerospace and Ocean Engineering, Virginia Polytechnic Inst. and State Univ., Blacksburg, VA, 1990.

[15]Fleming, J. L., Simpson, R. L., and Shinpaugh, K., "Further Investigation of the Near Wall Flow Structure of a Low Reynolds Number 3-D Turbulent Boundary Layer," AIAA Paper 95-0788, Jan. 1995.

[16]Ölçmen, S. M., and Simpson, R. L., "Some Effects of Pressure-Driven Three-Dimensionality on Higher Order Boundary Layer Turbulence," *Journal of Fluid Mechanics* (submitted for publication).

[17]Simpson, R. L., "Three-Dimensional Turbulent Boundary Layers and Separation," AIAA Paper 95-0226, Jan. 1995.

[18]Simpson, R. L., "Aspects of Turbulent Boundary-Layer Separation," *Progress in Aerospace Sciences*, Vol. 32, Nov. 1996, pp. 457–521.

[19]Lewis, D. J., "An Experimental Investigation of Heat Transfer in Three-Dimensional and Separating Turbulent Boundary Layers," Ph.D. Dissertation, Dept. of Aerospace and Ocean Engineering, Virginia Polytechnic Inst. and State Univ., Blacksburg, VA, 1996.

[20]Hager, J. M., Simmons, S., Smith, D., Onishi, S., Langley, L. W., and Diller, T. E., "Experimental Performance of a Heat Flux Microsensor," *Journal of Engineering for Gas Turbines and Power*, Vol. 113, No. 2, 1991, pp. 246–250.

[21]Bremhost, K., and Gilmore, D. B., "Influence of End Conduction on the Sensitivity to Stream Temperature Fluctuations of a Hot-Wire Anemometer," *International Journal of Heat and Mass Transfer*, Vol. 21, No. 2, 1978, pp. 145–154.

[22]Kays, W. M., and Crawford, M. E., *Convection Heat and Mass Transfer*, 2nd ed., McGraw–Hill, New York, 1980.

[23]Zaric, Z., "Wall Turbulence Structure and Convection Heat Transfer," *International Journal of Heat and Mass Transfer*, Vol. 18, No. 6, 1975, pp. 831–842.

[24]Nagano, Y., and Tagawa, M., "Statistical Characteristics of Wall Turbulence with a Passive Scalar," *Journal of Fluid Mechanics*, Vol. 196, Nov. 1988, pp. 157–185.

[25]Durst, F., Jovanovic, J., and Kanevce, L., "Probability Density Distribution in Turbulent Wall Boundary-Layer Flows," *Turbulent Shear Flows 5*, Springer–Verlag, Berlin, 1987, pp. 197–220.

[26]Brown, G. L., and Thomas, A. S. W., "Large Structure in a Turbulent Boundary Layer," *Physics of Fluids*, Vol. 20, No. 10, Pt. II, 1997, pp. S243–S252.

[27]Bagheri, N., Strataridakis, B. R., and White, B. R., "Turbulent Prandtl Number and Space–Time Temperature Correlation Measurements in an Incompressible Turbulent Boundary Layer," *AIAA Journal*, Vol. 30, No. 1, 1992, pp. 35–42.